



A three-dimensional microstructure-based photon-tracking model of radiative transfer in snow

T. U. Kaempfer,¹ M. A. Hopkins,¹ and D. K. Perovich¹

Received 9 November 2006; revised 16 August 2007; accepted 24 September 2007; published 28 December 2007.

[1] Solar radiation is a key component of the energy budget of snow-covered landscapes. Even a thin snow cover reflects most of the incident sunlight and transmits little. An understanding of the interaction of solar radiation with snow is essential to the study of the snow thermodynamics, chemistry, hydrology, ecology, and remote sensing. To investigate this interaction, a microstructure-based photon-tracking algorithm is presented. The three-dimensional snow microstructure is provided either by a discrete element model defined by shape, size, and spatial arrangement of individual ice grains or by an X-ray microtomography image of a snowpack. The model uses refraction, Fresnel reflection, and absorption laws, and the only optical input parameters are the complex index of refraction and absorption coefficient. The model follows individual photons through the microstructure, a porous network of ice and air, applying the fundamental optics laws at the ice-air interfaces and within the ice. By firing tens of thousands of photons a detailed examination of the spectral radiance and irradiance above, below, and within the snowpack is possible. The model was compared to results from a discrete ordinates model, and its sensitivity to the microstructural representation was studied. It was applied to investigate changes in reflected, absorbed, and transmitted light as a function of wavelength, snow depth, grain size, and snow density, used to predict the amount and direction of scattering within the snowpack, and used to explore the interaction of a collimated beam with snow.

Citation: Kaempfer, T. U., M. A. Hopkins, and D. K. Perovich (2007), A three-dimensional microstructure-based photon-tracking model of radiative transfer in snow, *J. Geophys. Res.*, 112, D24113, doi:10.1029/2006JD008239.

1. Introduction

[2] Snow is a highly scattering particulate medium with an intricate microstructure replete with air-ice interfaces that scatter light. Even a thin snow cover reflects most of the incident sunlight and transmits little. An understanding of the interaction of solar radiation with snow is an essential element to a diverse set of research areas including snow thermodynamics, chemistry, hydrology, ecology, and remote sensing. Solar radiation is a key component of the energy budget of snow [Barry, 1996; Nolin and Stroeve, 1997]. Detailed snow thermodynamic models require information on flux divergence with depth [Brandt and Warren, 1993; Beaglehole et al., 1998]. Spectral albedos and bidirectional reflectance distribution functions are needed to interpret visible and near-infrared remote sensing signatures [Hudson et al., 2006; Jin and Simpson, 2001; Warren et al., 1998]. The amount and spectral distribution of light transmitted through snow is of biological importance in both terrestrial and marine environments [McKenzie et al., 1998; Thomas and Duval, 1995; Smith et al., 1992]. There are a

host of photochemical processes that impact pollutant levels in snowpacks and in the atmosphere [Wolff et al., 2002].

[3] At visible and near infrared wavelengths, radiative transfer in snow is governed by two processes: absorption and scattering. As a ray of light passes through snow some of the light is absorbed by the ice and some of it is scattered in different directions. Absorption by ice is well understood and has a strong wavelength dependence [Grenfell and Perovich, 1981; Perovich and Govoni, 1991; Warren, 1984; Warren et al., 2006]. Scattering in snow results from differences in the real indices of refraction, n , between ice ($n \sim 1.31$) and air ($n \sim 1.0$). The real index of refraction of ice exhibits little wavelength dependence in the region of interest from 350 to 1400 nm [Warren, 1984] and typical snow grains are much larger than the wavelengths considered. Consequently, scattering does not vary appreciably with wavelength. However, scattering depends on the intricate and highly variable microstructure of snow. As snow is a highly scattering material it is difficult to directly measure the scattering coefficient and phase function. Moreover, the complex structure confounds theoretical estimates of snow scattering properties. Most theoretical work on scattering in snow has used a model snowpack consisting of spheres having the same density and specific surface area as the real snowpack [Grenfell and Warren, 1999; Grenfell et al., 2005; Neshyba et al., 2003].

¹Engineer Research and Development Center, Cold Regions Research and Engineering Laboratory, Hanover, New Hampshire, USA.

[4] There exists a wide array of snow radiative transfer models ranging from simple exponential decay to layer doubling to Monte Carlo to a detailed discrete ordinate multi-stream treatment of the equation of radiative transfer [Aoki *et al.*, 2000; Bohren and Barkstrom, 1974; Dunkle and Bevans, 1956; Leroux *et al.*, 1998; Mishchenko *et al.*, 1999; Stamnes *et al.*, 1988; Warren and Wiscombe, 1980; Wiscombe and Warren, 1980; Warren, 1982]. For the most part, the models take a continuum approach by assigning bulk optical properties to the medium. The models are usually plane-parallel and have multiple layers; that is, there is vertical variability in optical properties, but they assume that the layers are uniform in the horizontal direction. The continuum models do an excellent job in many applications, but are limited in their treatment of scattering and in the geometries they can investigate. To study the scattering at the individual ice crystal level, ray-tracing models are commonly used [Clarke *et al.*, 2006; Greenler, 1991; Hesse and Ulanowski, 2003; Macke *et al.*, 1996; Takano and Liou, 1995; Tape, 1994]. Such models have focused on the interaction of a ray of light with an individual, complex ice crystal. They use geometric optics to model reflections and refractions. The most advanced of these ray-tracing models also consider external diffraction by combining the geometric optics computations with Fraunhofer diffraction on the projected cross section of the object by explicitly solving the diffraction integral in the far-field approximation [e.g., Macke *et al.*, 1996; Takano and Liou, 1995] and edge diffraction by crystal facets using Monte Carlo techniques based on the Heisenberg uncertainty principle [Freniere *et al.*, 1999] or deduced from approximate relationships obtained from the exact half-plane diffraction theory calculations [Hesse and Ulanowski, 2003; Clarke *et al.*, 2006]. Snow, however, consists of a complex ice matrix of many sintered ice crystals and air filled pore space which prevents the direct application of single crystal models. Geometric optics models based on ray-tracing and Monte Carlo techniques have also been developed to study radiative transfer in spherical beds [Coquard and Baillis, 2005], light propagation in liquid foam represented by overlapping spherical bubbles [Swamy *et al.*, 2007], and fiber containing surfaces such as paper [Granberg *et al.*, 2003]. However, to our knowledge, no radiative transfer models accepting a versatile microstructural representation are available and have been used to study optical properties of snow.

[5] X-ray computed micro-tomography has emerged as a tool for snow observations at a scale relevant for the optics in the visible and near infrared wavelengths [Coléou *et al.*, 2001; Schneebeli *et al.*, 2004]. Time series of tomographic images of snow undergoing metamorphism have become available [Flin *et al.*, 2003; Schneebeli *et al.*, 2004]. In parallel, numerical models operating at the same microstructural scale are being developed, ranging from discrete element snow mechanics models [Johnson and Hopkins, 2005] to finite element heat transfer models [Kaempfer *et al.*, 2005] to initial approaches to model snow metamorphism [Flin *et al.*, 2003].

[6] We propose a snow radiative transfer model that takes as input a microstructural representation of snow either simulated by a discrete element model (DEM) or based on a tomographic image of natural snow. The model uses a geometric optics-based Monte Carlo technique to follow the

paths of individual photons through the porous network formed by the ice matrix, an ensemble of sintered snow grains, and the air filled pore space. Diffraction is neglected. The model has the capability to investigate various snowpack structures and geometries, ranging from simple spheres to cylinders with hemispherical ends for DEM structures, to explicit three-dimensional tomographic reproductions of snowpack geometry. For DEM structures, grain sizes and shapes, or a distribution thereof, can be selected as well as the snow density. The model is of particular value in examining the details of radiative transfer within the snowpack, examining near-surface light levels, exploring complex snow geometries, and deriving bulk scattering properties.

2. Model

2.1. Snow Representation

[7] Discrete element modeling is a technique for explicitly modeling the dynamics of assemblies of grains. It is particularly useful when a material undergoes large-scale discontinuous deformations that depend on microscale contact processes, internal breakage of contact bonds, and compaction of broken fragments. The DEM approach allows for the use of complex particle contact physics. The DEM stores the particle shapes, velocities, and locations, finds contacts, calculates forces and moments at each contact, calculates the conditions of contact bond formation, growth, and rupture, and calculates the movement of each particle within the aggregate [Johnson and Hopkins, 2005]. In particular, in the present context, by defining appropriate collision rules, the DEM can readily handle the interactions of a photon with the snow grains within an ice matrix. In other words, the photon tracking is performed using a DEM approach.

[8] The CRREL microstructural snow model (μ SNOW) is based on a DEM approach that uses axisymmetric particle shapes such as the cylinders with spherical ends shown in Figure 1. Various contact models are used to simulate unfrozen and frozen contacts between pairs of grains and to govern when and how quickly freezing occurs. In the current work model snow samples of various densities were created by placing particles with random orientation in a low-density array at the nodes of a three-dimensional cubic grid. The particles were spherical or cylindrical with hemispherical ends. Each particle was given random initial translational and rotational velocities. Following a method developed by Cundall and Strack [1979] space was contracted until the model snow reached the desired density. Whenever a particle contacted its neighbor a small frozen bond was instantaneously created and creep mechanisms relieved stress concentrations [Johnson and Hopkins, 2005]. This technique produced model snow samples that have considerable local spatial anisotropy as shown in the cross-sectional view in Figure 1. To be able to simulate a snowpack with infinite horizontal extent and arbitrary thickness, periodic samples were constructed by letting particles at one boundary interact with the particles at the opposite boundary. Samples were constructed with porosities ranging from 85% to 45% by successive space contractions. We used three sets of particles: spherical grains with constant radius $R = 0.5$ mm or $R = 0.1$ mm and

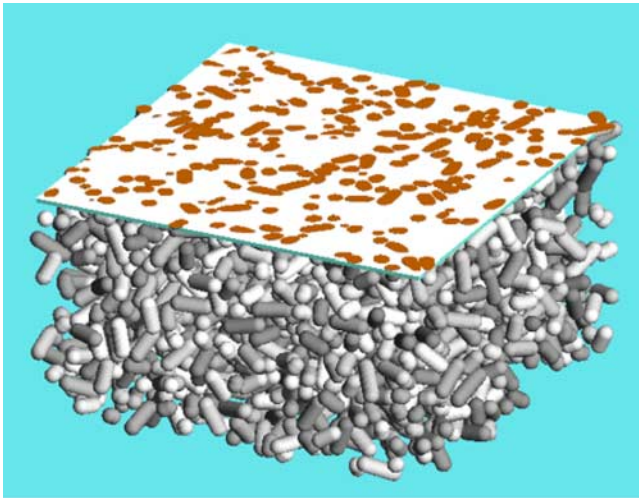


Figure 1. Cross-sectional slice through a DEM model snow sample with cylindrical snow grains having a porosity of 70%.

cylindrical particles with hemispherical ends with radius $R = 0.5$ mm and random size distribution of the cylinder length between 0 and $4R$, a cylinder with length 0 being a sphere with radius R . The samples were cubic with edge dimensions ranging from 32.9 mm at 85% porosity to 21.3 mm at 45% porosity and contained 4096 and 10200 particles for the cylindrical and spherical grains, respectively.

[9] The DEM model snow is ideal for studying the impact of physical properties such as mean grain size or density on the optical properties. However, the current DEM model is limited to regular particle shapes and it is still an open question how to accurately represent natural snow, which is not composed of spherical or cylindrical ice grains. For the

radiative transfer model to be more versatile and be applicable to experimentally imaged snow, a second representation of the snow microstructure was used. A universal representation of an arbitrary three-dimensional (3-D) microstructure is a binary voxel (3-D pixel) structure, where the voxel value is one for an ice- and zero for an air-voxel (Figure 2 (left)). This is typically the image format produced by an X-ray micro-tomography scan, with the voxels being of order 10–40 μm in size. However, a voxel representation is not well suited for optical computations due to the staggered, orthogonal ice-air interfaces. This limitation can be overcome by applying a Gaussian smoothing operation to the ice-air interface. By iteratively moving each vertex toward the geometric center of its neighboring vertices this method flattens out jagged interfaces. The degree of smoothness is controlled by the number of smoothing iterations. The resulting triangulated surface still represents the microstructural features as long as the initial voxel resolution was fine enough (Figure 2 (right)). The triangulation is defined such that each triangle has a unit normal pointing from ice to air. This allows us to determine from which medium a photon is approaching an interface before a collision. Note that by mirroring the voxel image in each direction and combining the results before the surface extraction and smoothing, we can construct a periodic model microstructure of the snow from a given sample.

2.2. Modeling Light Transmission Through Snow

[10] Light transmission through snow is governed by the absorption of light within the ice and scattering at the ice-air interfaces, the latter consisting of reflection, refraction, and diffraction. For snow, grain sizes are considerably larger than the wavelength in the visible and near-infrared region that we will consider here and geometric optics represent a reasonable approximation for solving the reflection and refraction problem within the snow. Application of geomet-

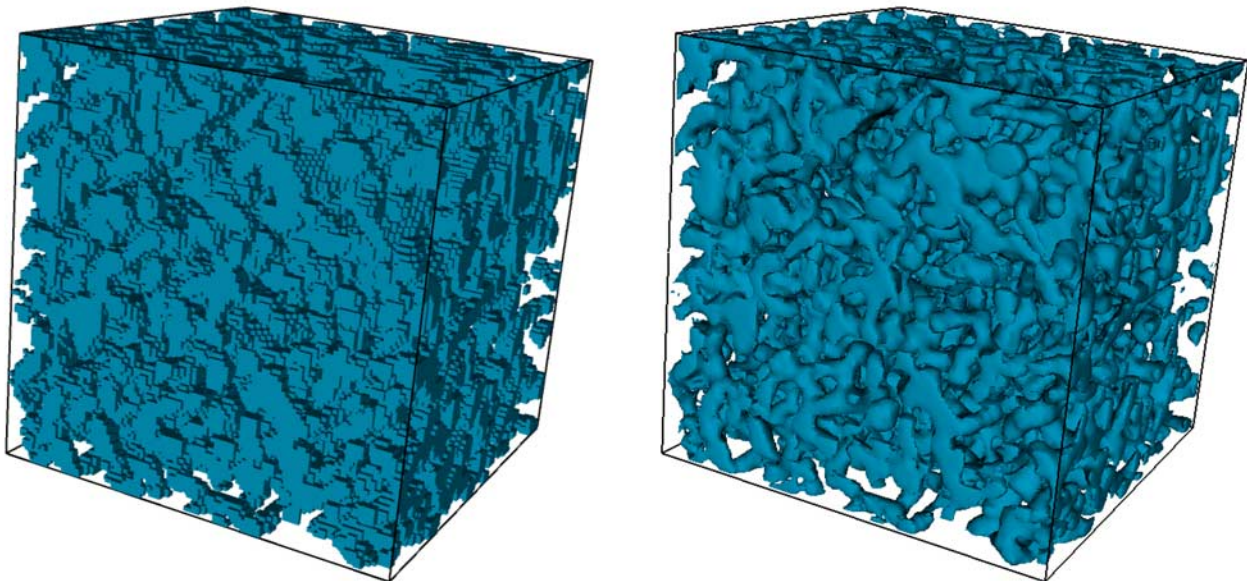


Figure 2. (left) Voxel representation and (right) corresponding triangulated and smoothed ice matrix surface for a tomographed snow sample. The snow consisted of small rounded grains and had a density of 170 kg m^{-3} . The voxel resolution is 40 μm , and the shown cube has a side length of 100 voxels or 4 mm.

ric optics implies the assumption that no small-scale surface structures exist. We will satisfy this criterion by considering aged, rounded grain snow structures in the present work. Note that this simplification also allows us to neglect edge diffraction by faceted crystals. However, external diffraction is still a concern since the extinction efficiency of a large (with respect to the wavelength) sphere is of order 2 and diffraction is thus important in contributing to forward scattering [Bohren and Huffman, 1983]. Unfortunately, the methods used to treat external diffraction for single crystals are based on the equivalent projected cross-sectional area of the particle, a concept which is at least computationally difficult to extend to a general porous medium such as the snow considered here. As a first step in this paper, we thus neglect any diffraction phenomena and limit our considerations to geometric optics together with absorption.

[11] There are two distinct approaches that can be used to explicitly model light transmission through the 3-D microstructure of snow. The first is to use a ray-tracing approach in which the bifurcation of a ray is modeled at each scattering event. The bifurcation represents the fact that at an ice-air interface part of the light is transmitted and part of it reflected. This approach produces a cascade of bifurcated rays that quickly grows computationally unmanageable especially at short wavelengths having low absorption. The obvious solution is to use some type of criteria to prune the bifurcations. The problem is that this leaves a significant fraction of indeterminate outcomes. The second approach is to fire individual photons sequentially and follow each one until it exits the top of the sample, exits the bottom of the sample, or is absorbed and terminated within an ice grain. This approach has the desirable feature that all outcomes are determinate. However, it does require a large number of photons, typically several tens of thousands.

[12] In the simulations discussed in this work light rays are modeled using the second approach. The discrete photons are treated as infinitesimal point particles. Each photon is fired with a specified direction and incidence angle at a point on the top of the model snow sample. As the photon travels through the snow sample it collides with grains. When it collides with a grain there are two possible outcomes. Either the photon is reflected or it is transmitted through the ice-air interface depending on a set of rules discussed below. A photon traveling through the interior of an ice grain may be absorbed with a probability that depends on the distance traveled and the wavelength assigned to the photon. As mentioned above, each photon has three possible fates: it may exit the top of the sample and be counted as reflected, exit the bottom of the sample and be counted as transmitted (i.e., the snow is supposed to be above a black surface), or be absorbed and terminated within an ice grain. Horizontally, the periodic boundary conditions imply an infinite extent. Photon motion through the model snow and in particular the collisions between photons and the ice matrix are handled using the discrete element framework, either using the snow grains (DEM model snow) or the triangles of the ice matrix surface (general microstructure) as collision candidates for the photon.

[13] To derive our geometric optics algorithm we begin by considering a ray of initial radiance I_i and incident zenith

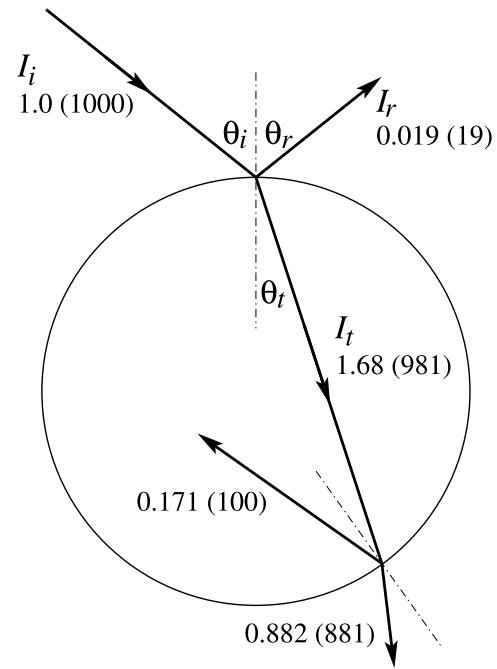


Figure 3. Schematic of ray tracing for an incident ray on a single grain. The real numbers refer to the radiance of the beam (equations (4)–(8)) at each step, while the integers in parentheses give the equivalence in whole photons at each step assuming that 1000 photons were in the original beam. Note that in this figure we neglected any absorption in the ice.

angle θ_i . The interaction of the ray with a single snow grain (see Figure 3) is governed by Snell's law, Fresnel's law, and the Bouguer-Lambert exponential absorption law. When a ray impinges on a snow grain some of the incident energy is reflected and some is transmitted. The angle of the reflected ray, θ_r , is equal to the angle of incidence, θ_i ,

$$\theta_r = \theta_i, \quad (1)$$

where the angles are measured relative to the surface normal at the collision point. The transmitted ray enters the medium at an angle θ_t defined by Snell's law such that

$$n_t \sin(\theta_t) = n_i \sin(\theta_i), \quad (2)$$

where n is the index of refraction and the subscripts i , t denote the incident medium and the medium that the photon enters, respectively. The angle of transmission is also measured relative to the surface normal at the collision point. The incident direction, reflected direction, transmitted direction, and surface normal vector are all coplanar. When colliding with an internal wall of an ice grain, there is a critical angle above which all the light is internally reflected. The critical angle, θ_c , is given by

$$\theta_c = \sin^{-1} \left(\frac{n_t}{n_i} \right). \quad (3)$$

Equations (1) and (2) define the angle of the reflected and transmitted beams. The radiance of the reflected beam, I_r , is

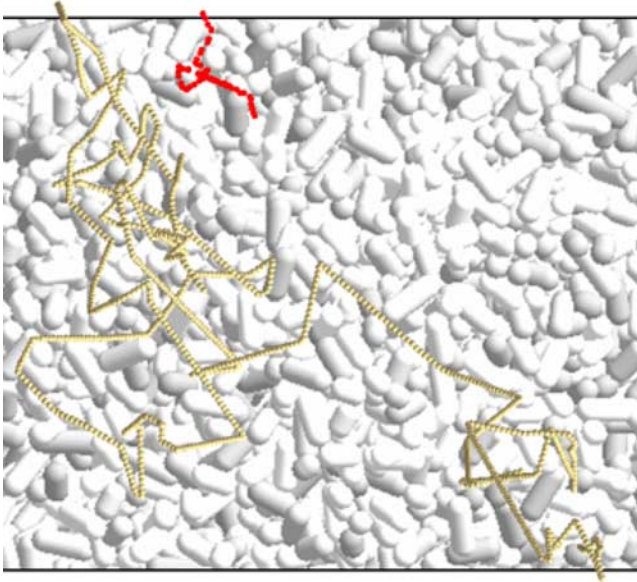


Figure 4. Schematic representation of photon tracking at 470 nm (yellow, long dotted line) and 1000 nm (red, short dotted line) through a cylindrical DEM snowpack.

determined from the incident radiance, I_i , by the Fresnel equation, which in simplified form reads

$$I_r(\theta_r) = I_i(\theta_i) \frac{1}{2} \left(\frac{\sin^2(\theta_i - \theta_t)}{\sin^2(\theta_i + \theta_t)} + \frac{\tan^2(\theta_i - \theta_t)}{\tan^2(\theta_i + \theta_t)} \right). \quad (4)$$

This applies for all angles with two exceptions. For angles greater than the critical angle θ_c we have

$$I_r(\theta_r) = I_i(\theta_i), \quad \forall \theta_i > \theta_c, \quad (5)$$

and for normal incidence ($\theta_i = 0$) we have

$$I_r(0) = I_i(0) \frac{(n_i - n_t)^2}{(n_i + n_t)^2}. \quad (6)$$

The radiance entering the other medium, I_t , is given by

$$I_t(\theta_t) = (I_i(\theta_i) - I_r(\theta_r)) \frac{n_t^2}{n_i^2}, \quad (7)$$

by Mobley [1994]. As a beam travels through the ice, it will be attenuated according to Beer's law. Suppose a beam travels a distance L during a time step Δt . Then the intensity at the end of the transit is

$$I(t + \Delta t) = I(t)e^{-kL}, \quad (8)$$

where k is the absorption coefficient at the wavelength of interest.

[14] At the level of individual photons these rules are implemented in a probabilistic sense. Each time a photon collides with an ice-air interface and at each time step when a photon travels through an ice grain a Monte Carlo-based

decision is made as to the fate of the photon. From equations (4), (5), and (6) we deduce the probability that a given photon that is colliding with the outer or inner surface of an ice grain will be reflected or transmitted. If we divide both sides of equation (4) by the incident radiance I_i the result I_r/I_i determines the fraction of the beam or incident photons that is reflected from the interface. The fate of one incident photon at an ice-air interface is determined by calculating I_r/I_i and then choosing a random number between 0 and 1. If the random number is less than I_r/I_i , then the photon is reflected, else it is transmitted with the appropriate refraction (equation (2)). If the photon is reflected its new direction of travel is given by

$$\mathbf{v}_r = \mathbf{v}_i - 2\mathbf{n}(\mathbf{v}_i \cdot \mathbf{n}), \quad (9)$$

where \mathbf{v}_i is the incident direction (velocity) of the photon and \mathbf{n} is the unit normal to the surface. If the photon is transmitted its new direction of travel is given by

$$\mathbf{v}_t = |\mathbf{v}_i| \left(\cos(\theta_t)\mathbf{n} + \sin(\theta_t) \frac{\mathbf{t}}{|\mathbf{t}|} \right), \quad (10)$$

where the angle of transmission θ_t is calculated from (2) and \mathbf{t} is perpendicular to \mathbf{n} in the direction given by

$$\mathbf{t} = \mathbf{v}_i - \mathbf{n}(\mathbf{v}_i \cdot \mathbf{n}). \quad (11)$$

If a photon is traveling a distance L through the interior of an ice grain during a given time step Δt , the probability of absorption, P_a , during Δt is determined by dividing (8) by $I(t)$ and subtracting the result from one:

$$P_a = 1 - \frac{I(t + \Delta t)}{I(t)} = 1 - e^{-kL}. \quad (12)$$

[15] Figure 4 schematically shows path of photons at wavelength of 470 nm and 1000 nm superimposed on a model snow sample. The short path length for 1000 nm is due to the large absorption coefficient (20.4 m^{-1}). At 470 nm, where the absorption coefficient is small ($5.23 \cdot 10^{-3} \text{ m}^{-1}$), the photon undergoes multiple scattering and usually emerges from the snowpack. Throughout the present work a value of 1.0 was used for the index of refraction of air and 1.30792 was used for ice. Absorption coefficients and e-folding distances for selected wavelengths are summarized in Table 1 [Grenfell and Perovich, 1981; Perovich and Govoni, 1991; Warren et al., 2006].

3. Results

[16] After comparison with a four-stream radiative transfer model, the photon-tracking model was used to explore the impact of solar incidence angle, wavelength, snow density, grain size, and snow depth on snow albedo, angular reflectance, transmittance, and depth-dependent absorption. In the simulations we focused primarily on thin snow covers, where the asymptotic albedo is not yet reached. Different snow depths were obtained by stacking multiple cubic samples in the vertical direction, taking advantage of the periodicity of the samples. If not otherwise noted, 20000

Table 1. Selected Wavelengths λ and Associated Absorption Coefficients k and e -Folding Length

λ , nm	k , m^{-1}	e -Fold l , m
350	$1.78 \cdot 10^{-3}$	561.8
390	$6.38 \cdot 10^{-4}$	1567.4
410	$8.18 \cdot 10^{-4}$	1222.5
450	$2.58 \cdot 10^{-3}$	387.6
470	$5.23 \cdot 10^{-3}$	191.2
550	$5.23 \cdot 10^{-2}$	19.1
600	0.12	8.3
650	0.28	3.62
800	2.10	0.476
900	5.86	0.171
1000	20.4	0.049
1030	28.4	0.035
1100	19.4	0.052
1170	41.2	0.024
1200	70.3	0.014
1330	125	0.008
1400	178	0.006

photons were fired for a given incidence angle and wavelength, since the albedo computations stabilized within less than 1% for 20000 or more photons. Each incident photon was initially placed at a given height z and random position (x, y) above the snow sample and assigned the desired incidence direction. Each photon had three possible fates. Photons that exited the top surface were counted as being reflected. Photons that exited the bottom surface were counted as being transmitted. The remaining photons were tracked until they were absorbed in the interior of the ice matrix.

3.1. Comparison With Discrete Ordinates Model

[17] We compared the results from the photon-tracking model with a four-stream discrete ordinates model (T. C. Grenfell, personal communication, 2005) for a sample case. While lacking in angular detail, four stream models produce reasonable values of irradiance and consequently albedo and transmittance [Grenfell, 1991]. For the four-stream model, we assumed a homogeneous snow layer with density 300 kg m^{-3} , a depth of 7.8 cm, and consisting of spherical grains with 0.5 mm radius over a black substrate. A one parameter Henyey-Greenstein phase function was used, with scattering parameters determined from Mie calculations. Photon-tracking model runs were performed for spherical particles with 0.5 mm radius and for a cylindrical particle distribution with radius $R = 0.5 \text{ mm}$ and random length between 0 and $4R$. These conditions are representative of a snowpack consisting of large, rounded grains. Figure 5 compares spectral albedos, absorptances, and transmittances for wavelengths varying between 400 and 1400 nm. The spectral shape between the models is in good agreement. In particular, at longer wavelengths, where the influence of grain size on albedo is more pronounced [Warren, 1982], the computed albedo for the spherical DEM particles is higher than that for cylindrical DEM particles whose equivalent sphere radius would be larger. The photon-tracking model computes a higher albedo and lower transmittance, especially at shorter wavelength, by approximately 10%. Even though this is a cumulative error (microstructural representation, limited amount of photons, physical model simplifications, etc.) it is consistent with the

omission of external diffraction, since diffraction by large particles is mainly in the forward direction [Bohren and Huffman, 1983] and tends thus to increase transmittance and consequently reduce the albedo.

3.2. Case Studies on Model Snow

[18] Considerable attention has been paid to the snow albedo and reflectance [Bourgeois et al., 2006; Gerland et al., 2000; Green et al., 2006; Grenfell and Perovich, 1981; Grenfell et al., 1994; Hall et al., 2002; Hudson et al., 2006; Kuhn, 1985; Nolin and Dozier, 2000; Painter et al., 2003; Vikhamar and Solberg, 2002; Wendler and Kelley, 1988] because of their importance to the calculation of the surface energy budget and interpretation of remotely sensed signatures. However, most of this work has focused on deep optically thick snowpacks. Figure 6 explores the impact of snow depth on albedo, absorptance, and transmittance for thin snow covers. Results are shown for different wavelengths representing cases with small and large amounts of absorption. In all cases the incident solar irradiance was represented as a direct beam at a zenith angle of 60° . The

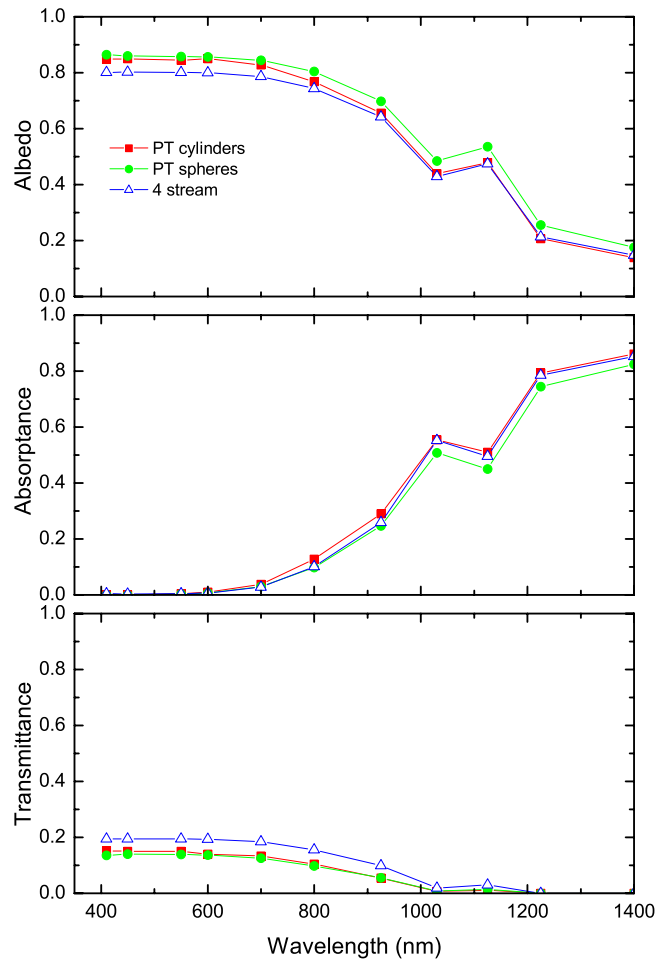


Figure 5. Comparison of DEM photon-tracking (PT) model to a four-stream discrete ordinates method continuum model. PT results are shown for both cylindrical and spherical particle shapes. The sample density was 300 kg m^{-3} , the snowpack thickness was 7.8 cm, and the incidence angle was 60° .

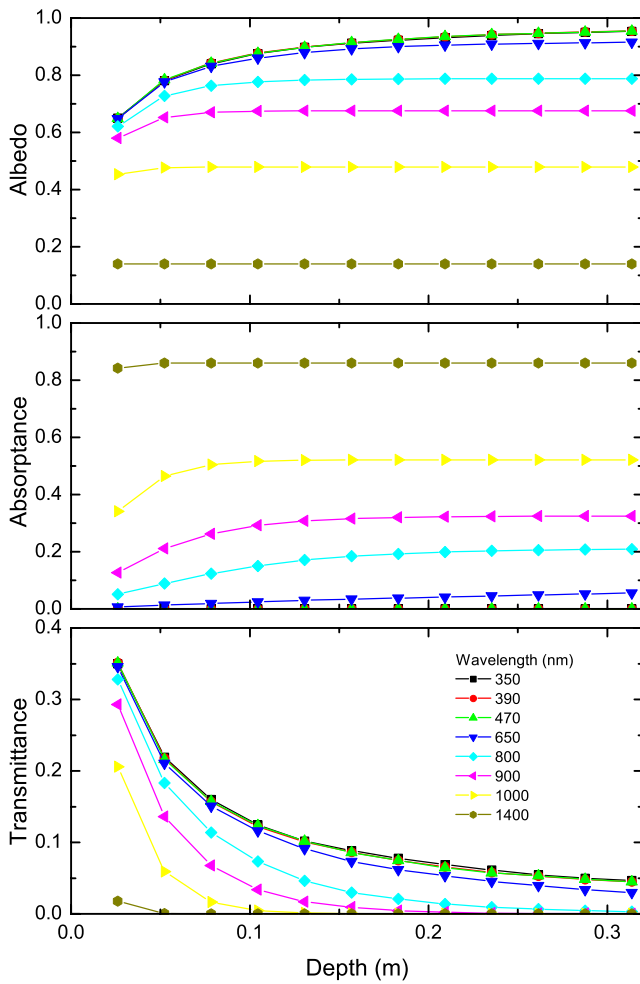


Figure 6. Reflected, absorbed, and transmitted photon fraction as a function of snow depth for thin snow covers. Results are shown for a density of 270 kg m^{-3} and cylindrical DEM particles. The incidence angle was 60° .

albedo shows a clear asymptotic increase with snow depth, where the asymptotic value is reached faster for longer wavelengths. The depth for a snowpack to be optically thick is thus less at longer wavelength, directly related to the increase of the absorption coefficient of ice with wavelength. The transmittance follows an exponential decrease with depth.

[19] Spectral absorptance as a function of depth is shown in Figure 7, the y axis showing the fraction of the photons that were absorbed in each layer. A 9.8 cm thick model snow sample composed of cylindrical particles and density equal to 140 kg m^{-3} was examined. The sample was divided into 25 equal layers and the number of photons that were absorbed in each layer was counted. Since we counted photons at each of these depth, a larger total number of photons, 250000, was needed for the results to stabilize and for the shortest wavelength with the lowest absorption coefficients even more photons would have been beneficial. The decay of the fraction of absorbed photons is exponential and low at 650 nm where the absorption coefficient of ice is smallest and high at 1400 nm where

the absorption coefficient is largest. At a given wavelength absorption is greatest near the surface and decreases with depth. At a wavelength of 1400 nm, 80% of the photons are absorbed in the top 3 cm of the snowpack and at longer wavelengths with greater absorption this fraction would be even larger.

[20] Earlier work [Wiscombe and Warren, 1980; Warren, 1982] established a clear relationship between snow grain size and optical properties. To investigate this relationship, we used a model snow of density 270 kg m^{-3} consisting of cylindrical particles. Using a simple scaling factor, varying between 0.1 and 1, we constructed ten samples having the same density but different grain sizes. Periodic boundary conditions were used to simulate a 10 cm thick snowpack, independent of the scaling factor. Reflected, absorbed, and transmitted photon fractions for different wavelengths are presented in Figure 8. Our results agree well with previous findings that smaller grains result in a higher albedo and less absorption. Moreover, the impact of grain size is greatest at longer wavelengths where the absorption coefficient of ice is large. Note that there is very little influence of the grain size on transmittance for all the studied wavelengths until the grains get large, with radius greater than approximately 0.4 mm.

[21] Less clear than the influence of grain size is the role of density on radiative properties of snow, mainly because it is difficult, in natural snow, to study density independently of other snow properties like the grain size and form. Using

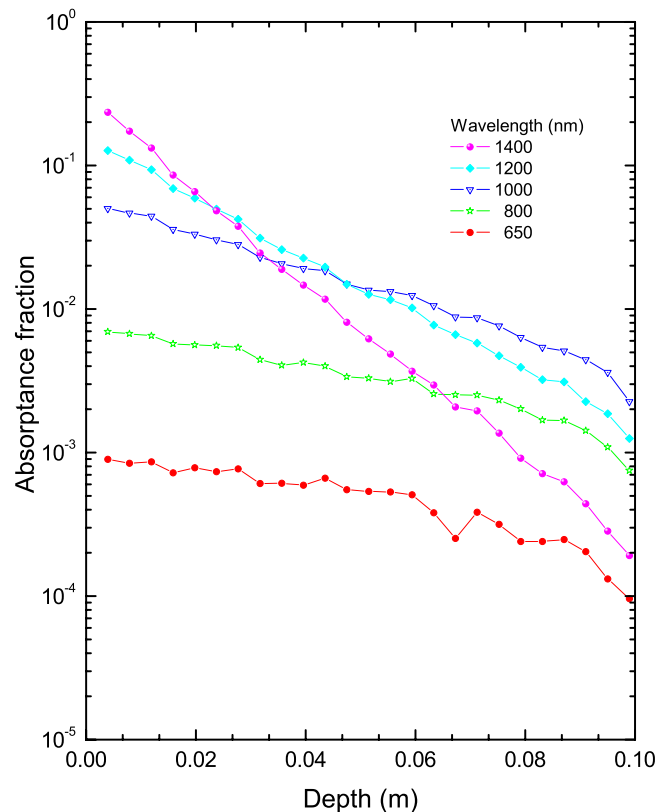


Figure 7. Fraction of absorbed photons in each 4-mm depth increment as a function of depth for a 9.8 cm thick snowpack with a density of 140 kg m^{-3} composed of cylindrical particles. The incidence angle was 50° .

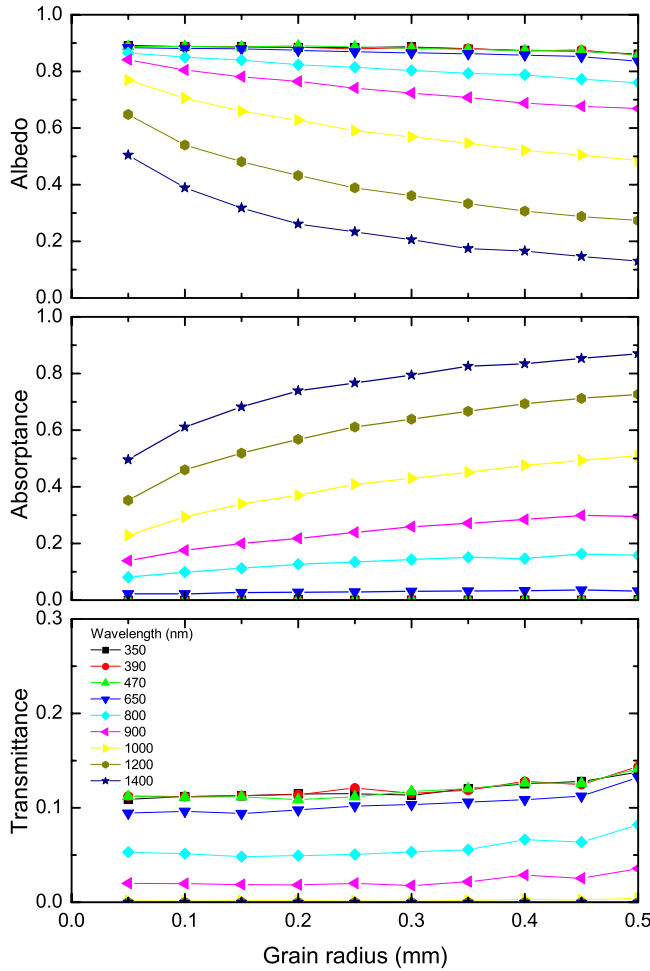


Figure 8. Reflected, absorbed, and transmitted photon fraction as a function of grain size for a thin snowpack of 10 cm height. Using a scaling of the DEM structure, the density of the snow sample was kept constant equal to 270 kg m^{-3} , while the cylindrical grains that had initially a radius of $R = 0.5 \text{ mm}$ and a length between 0 and $4R$ were successively downscaled to have radii between 0.5 and 0.05 mm. Results are shown for an incidence angle of 60° .

model snow samples with varying densities, but all constructed with the same cylindrical particles, we can circumvent this problem and simulate a densification or settling without grain size and form change. A model snow sample with cylindrical grains and a density of 136 kg m^{-3} was successively compressed in the vertical direction to reach higher densities up to 504 kg m^{-3} . Because of the compression, the height of the sample (and the depth of the simulated snowpack) diminished, keeping the water equivalent constant. Figure 9 presents the evolution of the reflected, absorbed, and transmitted photon fraction with density, respectively height, for an initial snowpack of 10 cm height. Our results confirm the common assumption that the density has very little effect on snow albedo [Bohren and Beshta, 1997]. We notice a very slight increase in transmittance together with a slight decrease in albedo for the highest densities, this effect being more pronounced at short wavelength, where absorption is close to zero.

[22] The photon-tracking model, with its ability to examine in detail the angular distribution of reflected light, is also well suited for studies related to the bidirectional reflectance distribution function (BRDF). The BRDF is formally defined by Nicodemus *et al.* [1977] as the ratio of the radiance, I_r [$\text{W m}^{-2} \text{ sr}^{-1}$], reflected into a particular direction, (θ_r, ϕ_r) , to the incident flux, F_0 [W m^{-2}], all of which is coming from a single direction, (θ_i, ϕ_i) :

$$BRDF(\theta_i, \phi_i, \theta_r, \phi_r) = \frac{I_r(\theta_i, \phi_i, \theta_r, \phi_r)}{F_0(\theta_i, \phi_i)}. \quad (13)$$

[23] In order to compare our results to measurements by Hudson *et al.* [2006] we will, instead of the BRDF, consider the anisotropic reflectance factor R defined as π times the ratio of radiance reflected into a particular direction to the reflected flux. R can be related to the BRDF by [Hudson *et al.*, 2006]:

$$R(\theta_i, \phi_i, \theta_r, \phi_r) = \frac{\pi}{\alpha} BRDF(\theta_i, \phi_i, \theta_r, \phi_r), \quad (14)$$

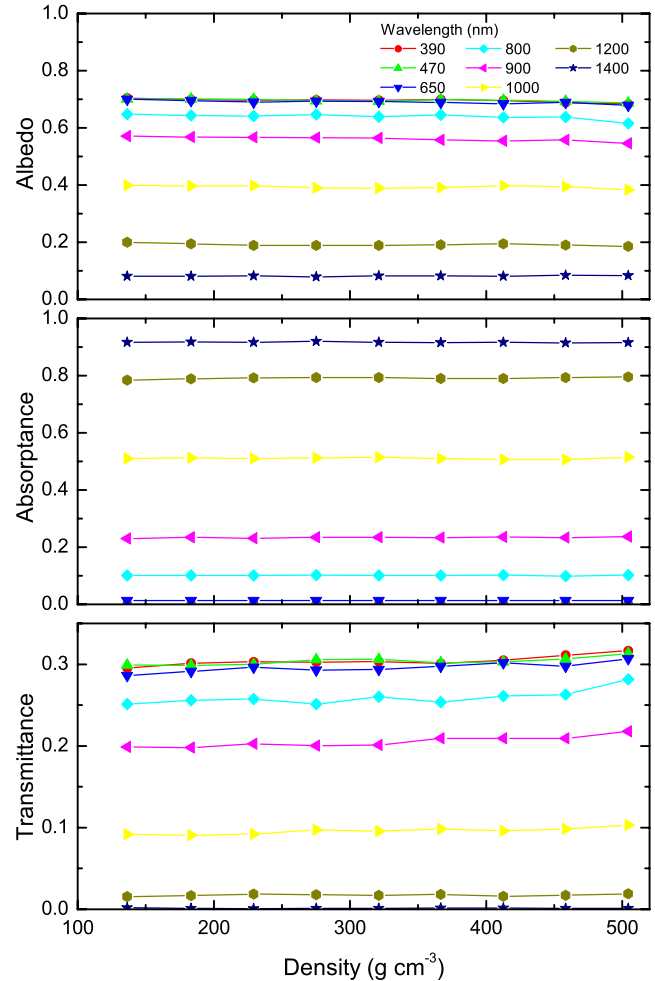


Figure 9. Reflected, absorbed, and transmitted photon fraction as a function of snow density for a thin snowpack with initial density of 136 kg m^{-3} and initial depth of 10 cm which was successively compressed to reach a density of 505 kg m^{-3} at a depth of 2.7 cm. The particles were cylindrical, and the incidence angle was 60° .

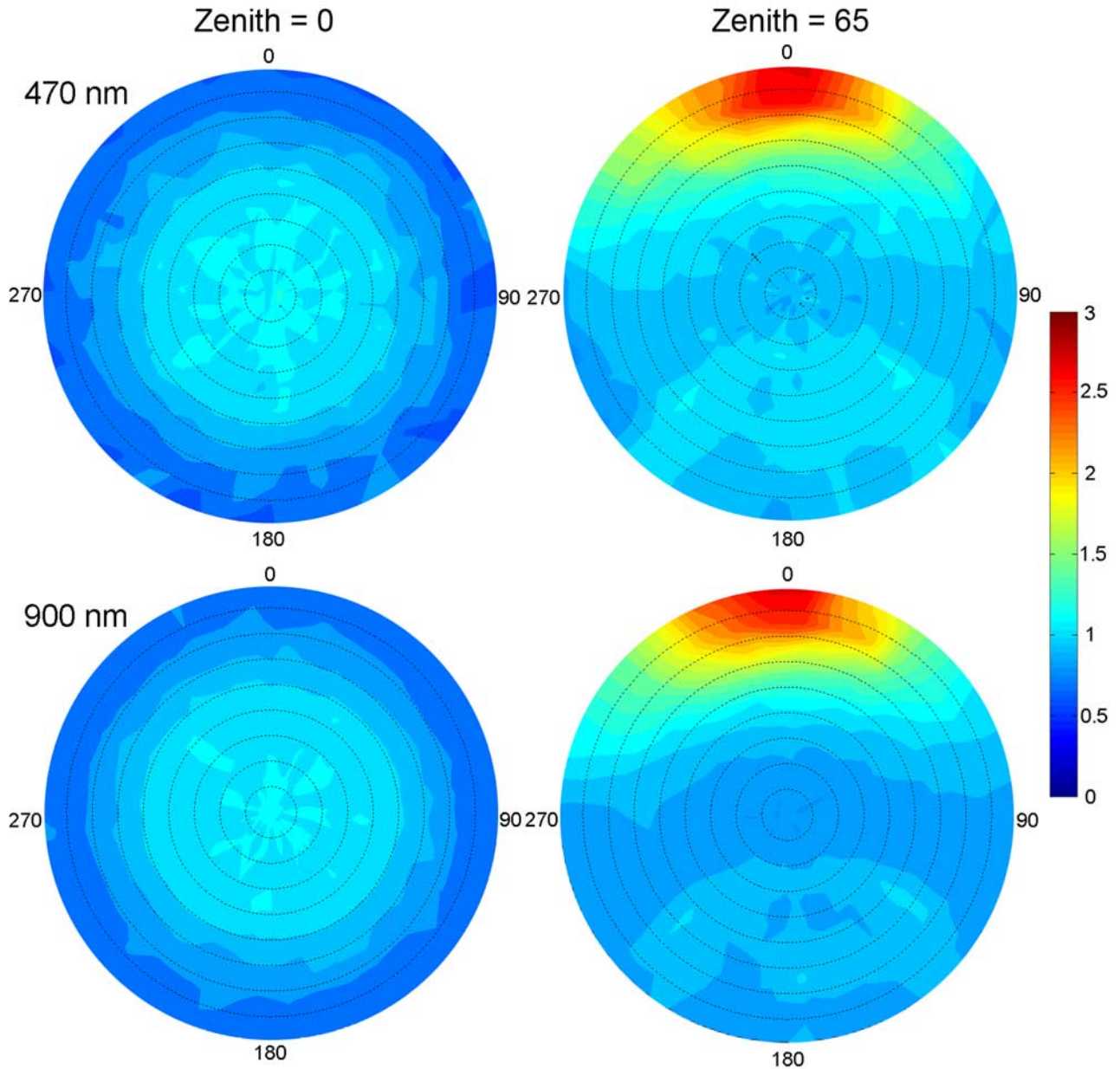


Figure 10. The directional-conical reflectance factor (DCRF) at 470 and 900 nm for incidence zenith angles of zero and 65°. The model was run on a spherical DEM model snowpack with grain radius of 0.1 mm, a density of 270 kg m^{-3} , and a depth of 30 cm.

where α is the albedo. Moreover, computational reasons impose the use of finite angular intervals rather than an infinite number of directions and we will compute the anisotropic directional-conical reflectance factor (DCRF) [Nicodemus et al., 1977; Schaepman-Strub et al., 2006] over an angular grid on the hemisphere with bin sizes of 10° in the zenith, θ , and azimuth, ϕ , directions using the definition of R integrated over the reflected directions (θ_r, ϕ_r) within this angular grid. In the photon-tracking model, the incident flux F_0 is equivalent to the number of photons fired, since we consider photons per unit surface area. To compute the radiance I_r , we note that [Nicodemus et al., 1977]

$$I_r = \frac{d^2\Phi}{dA \cos\theta d\omega}, \quad (15)$$

with Φ [W] being the radiant flux, ω [sr] the solid angle, and $A \cos\theta$ [m^2] the emission area A projected onto a plane perpendicular to the viewing direction (θ, ϕ) . I_r is thus obtained by summing the number of photons reflected into an angular bin $[\theta - \Delta\theta/2, \theta + \Delta\theta/2] \times [\phi - \Delta\phi/2, \phi + \Delta\phi/2]$, normalizing by the area of the bin (to obtain photons per steradian per emission area) and by $\cos\theta$ to obtain photons per steradian per projected area. DCRF results are shown for a model snow pack with spherical grains of radius 0.1 mm and 30 cm depth for 470 nm with 200,000 photons and for 900 nm with one million photons fired, for a collimated beam at solar zenith angles of zero and 65° (Figure 10). This case can represent the direct solar beam on a sunny day or the beam from a laser. A strong forward scattering peak is

observed for the 65° incidence angle, the anisotropy being lower at 470 nm, where the albedo is higher. This is consistent with measurements and discrete ordinates model computations in snow [e.g., Hudson et al., 2006; Middleton and Mungall, 1952; Painter and Dozier, 2004]. The case of 900 nm and 65° incidence angle corresponds to the measurements and simulations of Hudson et al. [2006, Figure 14]. For this case, our anisotropic DCRF ranges from 0.77 to 2.75 sr^{-1} . The maximum value is lower by ca. 20% than the simulation with the discrete ordinates model DISORT [Stamnes et al., 1988], however higher than the observations for the natural rough snow surface. One reason might be that our model considers microstructural surface roughness in the snow representation, lying between the rough surface observations and the smooth surface DISORT simulation. Another source of error could be the neglected external diffraction, which enhances forward scattering.

3.3. Voxel Structures

[24] The present photon-tracking model is not limited to microstructures formed by an ensemble of regular grains, but can be applied to any triangulated surface representing a complex matrix of ice-air interfaces in snow. If the input is formed by regular grains, the ice-air interfaces, being the grain surfaces, are always smooth. This is not necessarily true for an arbitrary triangulated representation of a microstructure. Since the fate of the photons in the model depends largely on the optical laws at ice-air interfaces and in particular on the angle between the travel direction of the photon and the interface normal, this is a critical aspect. Starting from a versatile 3-D binary voxel representation of a given microstructure, the goal is thus to extract the ice-air interface which represents as close as possible the initial (smooth and nonvoxelized) ice-air interface. We studied the influence of the surface definition on the simulation results by applying the model to a given DEM model snow (constructed using the usual cylindrical grains) and using the following microstructural representations (see Figure 11): the DEM particle representation; a smooth triangulation of the DEM particle surfaces; and a 3-D voxel image of the model snow. The 3-D voxel image was obtained by overlaying the sample with a cubic grid and determining whether the center of each cell or voxel was in ice (inside a particle) or in air (outside all particles). The surface of the voxel image was then triangulated and smoothed by a Gaussian smoothing operation with a variable number of iterations.

[25] A key parameter in the microstructural representation is the resolution of the voxel image and it is natural to require the model to well represent the density. For our large grained DEM snow, the difference in densities between a voxel resolution of 150 and 200 per 2.6 cm was less than 2%. For computational reasons we chose the rather rough 150 resolution ($175 \mu\text{m}$ voxel size). The resolution for images of natural snow is determined by the tomography equipment. Tomography-based numerical simulations showed that if a microstructural feature is resolved by four or more voxels, physical properties like stress and strain or heat conductivity can be predicted with an error smaller than 2% [van Rietbergen et al., 1995; Kaempfer et al., 2005]. Note that our chosen resolutions meet this criterion.

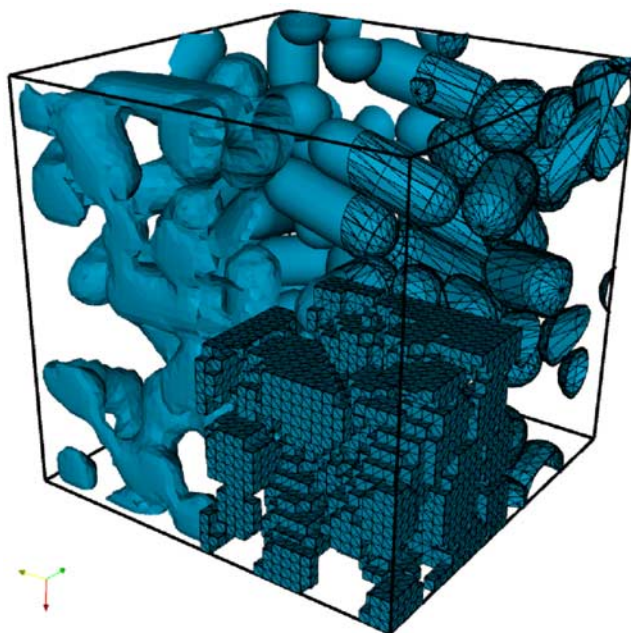


Figure 11. Different three-dimensional representations of a model snow sample: Cylindrical grains DEM representation (upper back corner), cylindrical grains with triangulated surface (right, back), 3-D voxel representation with triangulated ice-air interface (bottom, front), and voxel-based triangulation after smoothing, here with 200 Gaussian smoothing iterations (left). The DEM grains had a radius of 0.5 mm, and the side length of the whole shown cube corresponds to 40 voxels of $175 \mu\text{m}$ side length, thus to 7 mm.

[26] The reflected, absorbed, and transmitted photon fraction was computed for the different microstructural representations of the model snow with cylindrical grains, a density of 270 kg m^{-3} , and a snow depth of 2.6 cm (Figure 12). The results for the DEM particle representation and its smooth triangulation are nearly coincident. However, an only slightly smoothed triangulation of the voxelized structure significantly overestimates the albedo and underestimates the transmittance. This is likely due to many nearly orthogonal planes and their preferred orientations. As smoothing of the ice-air interface proceeds, we approach the DEM results. For 400 smoothing iterations, the results agree to within approximately 5% and the remaining discrepancy might be explained by differences in the microstructures which are created during the voxelization such as for example a change in bond geometry between grains or by a slight shrinkage of the ice matrix due to the Gaussian smoothing algorithm.

3.4. Application to Natural Snow

[27] We applied the photon-tracking model to the microstructure of a natural snowpack whose representation was obtained by microtomography. The snow was collected in the field (February 2006, Davos, Switzerland) and stored in a $30 \times 30 \times 30 \text{ cm}^3$ Styrofoam box at isothermal conditions of -3°C for 17 days. A cylindrical subsample with a radius of 33.5 mm and a height of 65 mm was extracted horizon-

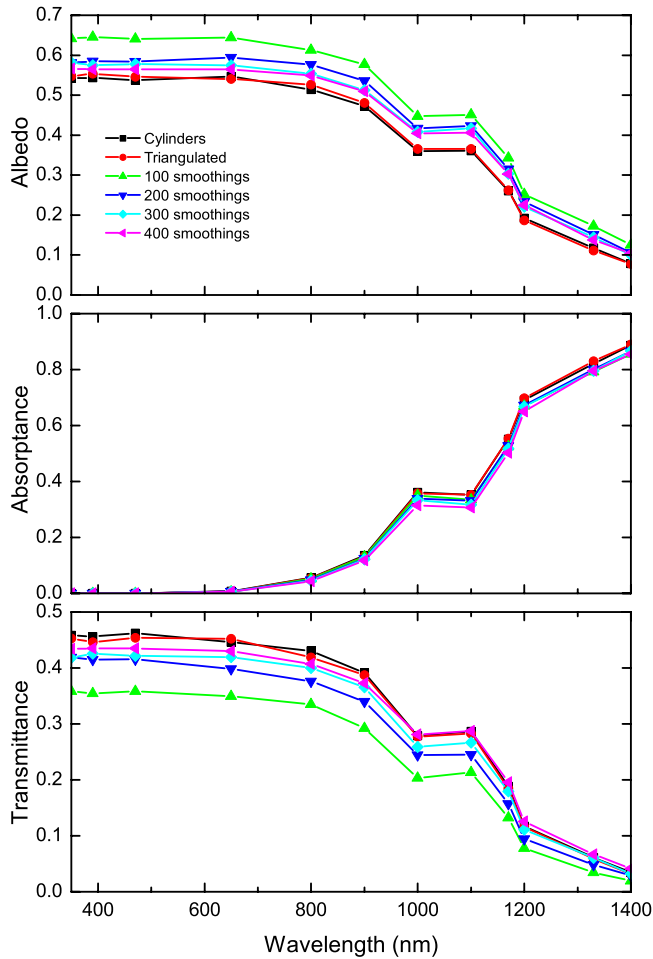


Figure 12. Reflected, absorbed, and transmitted photon fraction for a 2.6 cm thick model snowpack with cylindrical grains of density 270 kg m^{-3} and an incidence angle of 15° . Shown are the computations using the DEM particle representation, the direct triangulation of those particles, and the voxel-based ice-air interface after Gaussian smoothing with 100, 200, 300, and 400 smoothing iterations.

tally and measured with an X-ray microtomograph at a resolution of $10 \mu\text{m}$. The images were filtered with a $3 \times 3 \times 3$ median filter and segmented using a constant threshold to produce a binary image of the snow microstructure (Figure 2). To reduce data size, the resolution was scaled up to $40 \mu\text{m}$ and a subdomain of $100 \times 100 \times 100$ voxels ($4 \times 4 \times 4 \text{ mm}$) was extracted from the image. This subdomain was mirrored along each axis to produce an $8 \times 8 \times 8 \text{ mm}$ periodic cell representing the snow microstructure. The surface of the ice matrix was extracted, triangulated, and smoothed by a Gaussian smoothing operation with 400 iterations. The resulting triangulation was used for the photon-tracking computations. The periodic images created an effectively infinite horizontal extent while the effective thickness of the snow sample, obtained by stacking periodic images, was 30 cm. The absorbed, reflected, and transmitted photon fraction was computed for an incident beam at 60° (Figure 13). The computed apparent optical properties of the

snow sample show the expected qualitative behavior, with an albedo very close to one at shorter wavelength.

4. Discussion

[28] Using only two fundamental optical parameters, namely the complex index of refraction and the absorption coefficient of ice, our microstructure-based optical model produces consistent results with respect to available conceptual models of the sensitivities of snow optical properties. The simplicity of the optical treatment based on a few fundamental laws comes at a certain price: not only density and grain size, but an accurate representation of the snow microstructure at the scale of $10\text{--}100 \mu\text{m}$ is needed. Together with the large number of photons necessary to simulate a light source, this makes for a computationally intensive model. Because of this it is not appropriate for simple applications such as determining albedo for an optically thick snow cover with uniform diameter spherical grains. Its strengths are in treating complex geometries and examining scattering in great detail. It is particularly effective in examining the details of the spectral radiance field

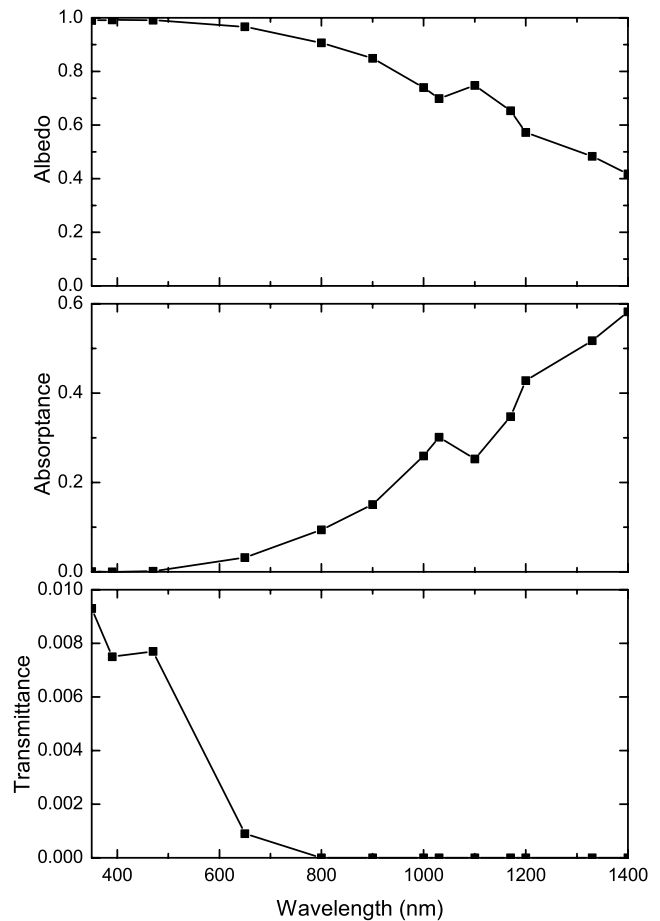


Figure 13. Reflected, absorbed, and transmitted photon fraction as a function of wavelength for a natural snowpack with a density of 175 kg m^{-3} and a thickness of 30 cm computed for an incidence angle of 60° . The computations used the microstructural input from an X-ray microtomography image of the snow.

both within and outside the snowpack. Applications include snow photochemistry studies, heat budget calculations, and interpretation of optical remote sensing signatures.

[29] We compared the model to a four stream discrete ordinates model and the spectral shapes are in good agreement. We note that the photon-tracking results for cylindrical grains (with larger equivalent sphere radius) agree better with the four stream results at larger wavelength. The spherical computations overestimate the albedo and underestimate the transmittance by approximately 10% over the whole wavelength range. It could be that the four streams in the discrete ordinates model were a too rough approximation for the thin snow cover considered and a more sophisticated radiative transfer model like DISORT [Stamnes *et al.*, 1988] will have to be considered for a sound model validation. Note however that the trend of the difference between the two models is consistent with the omission of external diffraction in the photon-tracking model, since diffraction would contribute to forward scattering, thus deeper penetration of light into the snowpack, and consequently a lower albedo.

[30] The photon-tracking model predicts well the dependencies of albedo, absorption, and transmittance on snow depth (Figures 6 and 7) and grain size (Figure 8). Moreover, using the DEM model snow, the influence of parameters that are impossible to isolate in natural snow can be studied, such as the evolution of optical properties with density at constant grain sizes (Figure 9). For the model snow we can confirm the hypothesis that there is very little dependence of the albedo on snow density [Bohren and Beshta, 1997]. A slight decrease in albedo together with an increase in transmission becomes visible at very high densities, which might be associated with a decrease in scattering events as the snow approaches pure ice.

[31] An examination of the angular distribution of reflected light is straightforward and makes the photon-tracking model ideal for studies related to the bidirectional reflectance distribution function (Figure 10). To produce smooth results, a large number of photons has to be fired as can be seen when passing from 200,000 photons at 470 nm to one million photons at 900 nm. When comparing our computed DCRF to published measurements and simulations by Hudson *et al.* [2006, Figure 14], we find good agreement for the angular distribution of the reflectance factor, in particular the presence of a strong forward scattering peak. Absolute DCRF values differ between the numerical simulations by up to 20%, possibly because of some surface roughness in the photon-tracking model or the neglected external diffraction. Applications with respect to the angular distribution could consist in characterizing the photons that contribute to the forward scattering peak. For example, using a similar model than ours, Granberg *et al.* [2003] showed that in sheets of paper containing hollow fibers, the forward scattering peak is mainly due to photons reflected from the inner fiber surfaces.

[32] When the photon-tracking model is applied to voxel-based microstructures, special care has to be taken with respect to the microstructural representation (Figure 12). In particular, a pure voxel-based treatment consists of orthogonal planes of the ice-air interface that distorts photon-tracking results. Our results indicate that a Gaussian smoothing procedure with several hundred iterations is

sufficient to render the ice-air interfaces smooth enough for the model to generate accurate results. More sophisticated smoothing algorithms might be considered in the future since Gaussian smoothing can lead to some shrinkage of the structure.

[33] The application of the photon-tracking model to the microstructure of a natural, isothermally metamorphosed snowpack as obtained by microtomography gives apparent optical properties qualitatively consistent with measurements and shows the feasibility of our approach. The model computes an albedo very close to one at shorter wavelength, which is not always observed and possibly due to impurities in natural snow. Impurities like soot particles might be added to the model by placing small black spheres with high absorption coefficients inside the microstructural representation. Another model extension could be the inclusion of liquid water.

[34] So far, the photon-tracking model uses geometric optics and neglects any diffraction phenomena. The model results are qualitatively consistent with observations or other simulations for snow. Cumulative errors of approximately 10% for flux computations like transmission and albedo and 20% for absolute values of reflectance factors are observed. The trends of these errors are consistent with the omission of external diffraction. At the moment we are unable to determine how much of the errors are due to the neglected physics and how much to the other numerical approximations in the photon-tracking model such as the microstructural snow representation or the limited number of photons fired. In the future, a thorough validation campaign using experimental optical measurements, together with 3-D microstructural snow characterizations and successive photon-tracking computations will be conducted and improve our understanding of the link between snow microstructure and optics.

5. Conclusion

[35] The presented snow microstructural photon-tracking model is a powerful tool for examining radiative transfer in snow. The strengths of the model are in treating complex geometries and examining scattering in detail. Non-plane parallel and irregularly shaped geometries can be investigated. The three-dimensional structure of an actual snowpack can be assimilated into the model. A “grain by grain” analysis of the interaction of solar radiation with snow can be performed. Such an analysis is particularly valuable in studies of snow photochemistry. The photon-tracking radiative transfer formulation is embedded in a discrete element model of snowpack microstructure. New capabilities are being added to the microstructure model so that it can treat snow metamorphism and melt water in the snowpack. With each such addition, its radiative transfer capabilities are thus extended implicitly. Moreover, the radiative transfer model accepts input from modern snow microstructure observational techniques like X-ray-computed microtomography. As time-lapse series of metamorphosing snow become available, the radiative transfer properties and their evolution during metamorphism can be studied in detail. Future work will consist in a thorough model validation including assessment of diffraction phenomena, a model extension to include diffraction, and the application of the model to

metamorphosing snowpacks. Inclusions of impurities in the model are also envisaged.

[36] **Acknowledgments.** The authors thank T. C. Grenfell for his helpful suggestions and for contributing the four-stream results used for comparison; M. Schneebeli and B. Pinzer, SLF Davos, Switzerland, for the tomographic snow microstructural data; T. Painter and three anonymous reviewers for their useful suggestions for revisions that helped improve the paper. This work has been funded by the Department of the Army AT-59 program and has been supported in part by an appointment to the Research Participation Program at the USACRREL administered by the Oak Ridge Institute for Science and Education through an interagency agreement between the U.S. Department of Energy and USACRREL.

References

- Aoki, T., T. Aoki, M. Fukabori, A. Hachikubo, Y. Tachibana, and F. Nishio (2000), Effect of snow physical parameters on spectral albedo and bidirectional reflectance of snow surface, *J. Geophys. Res.*, *105*, 10,219–10,236.
- Barry, R. G. (1996), The parameterization of surface albedo for sea ice and its snow cover, *Prog. Phys. Geogr.*, *20*, 63–79.
- Beaglehole, D., B. Ramanathan, and J. Rumberg (1998), The UV to IR transmittance of Antarctic snow, *J. Geophys. Res.*, *103*, 8849–8857.
- Bohren, C. F., and B. R. Barkstrom (1974), Theory of the optical properties of snow, *J. Geophys. Res.*, *79*, 4527–4535.
- Bohren, C. F., and R. L. Bescht (1997), Snowpack albedo and snow density, *Cold Reg. Sci. Technol.*, *1*, 47–50.
- Bohren, C. F., and D. R. Huffman (1983), *Absorption and Scattering of Light by Small Particles*, 530 pp., John Wiley, Hoboken, N. J.
- Bourgeois, C. S., P. Calanca, and A. Ohmura (2006), A field study of the hemispherical directional reflectance factor and spectral albedo of dry snow, *J. Geophys. Res.*, *111*, D20108, doi:10.1029/2006JD007296.
- Brandt, R. E., and S. G. Warren (1993), Solar-heating rates and temperature profiles in Antarctic snow and ice, *J. Glaciol.*, *39*, 99–110.
- Clarke, A. J. M., E. Hesse, Z. Ulanowski, and P. H. Kaye (2006), A 3D implementation of ray tracing combined with diffraction on facets: Verification and a potential application, *J. Quant. Spectrosc. Radiat. Transfer*, *100*, 103–114.
- Coléou, C., B. Lesaffre, J.-B. Brzoska, W. Ludwig, and E. Bollor (2001), Three-dimensional snow images by X-ray microtomography, *Ann. Glaciol.*, *32*, 75–81.
- Coquard, R., and D. Baillis (2005), Radiative characteristics of beds made of large spheres containing an absorbing and scattering medium, *Int. J. Thermal Sci.*, *44*, 926–932, doi:10.1016/j.ijthermalsci.2005.03.009.
- Cundall, P. A., and O. D. L. Strack (1979), A discrete numerical model for granular assemblies, *Geotechnique*, *29*, 47–65.
- Dunkle, R. V., and J. T. Bevans (1956), An approximate analysis of the solar reflectance and transmittance of a snow cover, *J. Meteorol.*, *13*, 212–216.
- Flin, F., J. B. Brzoska, B. Lesaffre, C. Coléou, and R. A. Pieritz (2003), Full three-dimensional modelling of curvature-dependent snow metamorphism: First results and comparison with experimental tomographic data, *J. Phys. D Appl. Phys.*, *39*, A49–A54.
- Freniere, E. R., G. G. Gregory, and R. A. Hassler (1999), Edge diffraction in Monte Carlo ray tracing, *Proc. SPIE Int. Soc. Opt. Eng.*, *3780*, 151–157.
- Gerland, S. J., G. E. Liton, J. G. Winther, J. B. Oerback, and B. V. Ivanov (2000), Attenuation of solar radiation in Arctic snow: Field observations and modeling, *Ann. Glaciol.*, *31*, 364–368.
- Granberg, H., J. Jensen, and L. Mattsson (2003), Forward scattering of fibre-containing surfaces studied by 3-D reflectance distribution simulations and measurements, *Opt. Eng.*, *42*, 2384–2390.
- Green, R. O., T. H. Painter, D. A. Roberts, and J. Dozier (2006), Measuring the expressed abundance of the three phases of water with an imaging spectrometer over melting snow, *Water Resour. Res.*, *42*, W10402, doi:10.1029/2005WR004509.
- Greenler, R. (1991), *Rainbows, Halos, and Glories*, Cambridge Univ. Press, 195 pp., Cambridge, U. K.
- Grenfell, T. C. (1991), A radiative transfer model for sea ice with vertical structure variations, *J. Geophys. Res.*, *96*, 16,991–17,001.
- Grenfell, T. C., and D. K. Perovich (1981), Radiation absorption coefficients of polycrystalline ice from 400–1400 nm, *J. Geophys. Res.*, *86*, 7447–7450.
- Grenfell, T. C., and S. G. Warren (1999), Representation of a nonspherical ice particle by a collection of independent spheres for scattering and absorption of radiation, *J. Geophys. Res.*, *104*, 31,697–31,709.
- Grenfell, T. C., S. G. Warren, and P. C. Mullen (1994), Reflection of solar radiation by the Antarctic snow surface at ultraviolet, visible, and near-infrared wavelengths, *J. Geophys. Res.*, *99*, 18,669–18,684.
- Grenfell, T. C., S. P. Neshyba, and S. G. Warren (2005), Representation of a nonspherical ice particle by a collection of independent spheres for scattering and absorption of radiation: 3. Hollow columns and plates, *J. Geophys. Res.*, *110*, D17203, doi:10.1029/2005JD005811.
- Hall, D. K., G. A. Riggs, V. V. Salomonson, N. E. DiGirolamo, and K. J. Bayr (2002), MODIS snow-cover products, *Remote Sens. Environ.*, *83*, 181–194.
- Hesse, E., and Z. Ulanowski (2003), Scattering from long prisms computed using ray tracing combined with diffraction on facets, *J. Quant. Spectrosc. Radiat. Transfer*, *79–80*, 721–732.
- Hudson, S. R., S. G. Warren, R. E. Brandt, T. C. Grenfell, and D. Six (2006), Spectral bidirectional reflectance of Antarctic snow: Measurements and parametrization, *J. Geophys. Res.*, *111*, D18106, doi:10.1029/2006JD007290.
- Jin, Z., and J. J. Simpson (2001), Anisotropic reflectance of snow observed from space over the Arctic and its effect on solar energy balance, *Remote Sens. Environ.*, *75*, 63–75.
- Johnson, J. B., and M. A. Hopkins (2005), Identifying microstructural deformation mechanisms in snow using discrete-element modeling, *J. Glaciol.*, *51*, 432–442.
- Kaempfer, T. U., M. Schneebeli, and S. A. Sokratov (2005), A microstructural approach to model heat transfer in snow, *Geophys. Res. Lett.*, *32*, L21503, doi:10.1029/2005GL023873.
- Kuhn, M. (1985), Bidirectional reflectance of polar and alpine snow surfaces, *Ann. Glaciol.*, *6*, 164–167.
- Leroux, C., J.-L. Deuzé, P. Goloub, C. Sergent, and M. Fily (1998), Ground measurements of the polarized bidirectional reflectance of snow in the near-infrared spectral domain: Comparisons with model results, *J. Geophys. Res.*, *103*, 19,721–19,731.
- Macke, A., J. Mueller, and E. Raschke (1996), Single scattering properties of atmospheric ice crystals, *J. Atmos. Sci.*, *53*, 2813–2825.
- McKenzie, R. L., K. J. Paulin, and S. Madronich (1998), Effects of snow cover on UV irradiance and surface albedo: A case study, *J. Geophys. Res.*, *103*, 28,785–28,792.
- Middleton, W. E. K., and A. G. Mungall (1952), The luminous directional reflectance of snow, *J. Opt. Soc. Am.*, *42*, 572–579.
- Mishchenko, M. I., J. M. Dlugach, E. G. Yanovitskij, and N. T. Zakharova (1999), Bidirectional reflectance of flat, optically thick particulate layers: An efficient radiative transfer solution and applications to snow and soil surfaces, *J. Quant. Spectrosc. Radiat. Transfer*, *63*, 409–432.
- Mobley, C. D. (1994), *Light and Water*, 592 pp., Academic, San Diego, Calif.
- Neshyba, S. P., T. C. Grenfell, and S. G. Warren (2003), Representation of a nonspherical ice particle by a collection of independent spheres for scattering and absorption of radiation: 2. Hexagonal columns and plates, *J. Geophys. Res.*, *108*(D15), 4448, doi:10.1029/2002JD003302.
- Nicodemus, F. E., J. C. Richmond, and J. J. Hsia (1977), *Geometrical Considerations and Nomenclature for Reflectance*, NBS Monogr., vol. 160, U.S. Dep. of Comm., Natl. Bur. of Stand., Gaithersburg, Md.
- Nolin, A. W., and J. Dozier (2000), A hyperspectral method for remotely sensing the grain size of snow, *Remote Sens. Environ.*, *74*, 207–216.
- Nolin, A. W., and J. Stroeve (1997), The changing albedo of the Greenland ice sheet: Implications for climate modeling, *Ann. Glaciol.*, *25*, 51–57.
- Painter, T. H., and J. Dozier (2004), Measurements of the hemispherical-directional reflectance of snow at fine spectral and angular resolution, *J. Geophys. Res.*, *109*, D18115, doi:10.1029/2003JD004458.
- Painter, T. H., J. Dozier, D. A. Roberts, R. E. Davis, and R. O. Green (2003), Retrieval of subpixel snow-covered area and grain size from imaging spectrometer data, *Remote Sens. Environ.*, *85*, 64–77.
- Perovich, D. K., and J. W. Govoni (1991), Absorption coefficients of ice from 250 to 400 nm, *Geophys. Res. Lett.*, *18*, 1233–1235.
- Schaepman-Strub, G., M. E. Schaepman, T. H. Painter, S. Dangel, and J. V. Martonchick (2006), Reflectance quantities in optical remote sensing: Definitions and case studies, *Remote Sens. Environ.*, *103*, 27–42, doi:10.1016/j.rse.2006.03.002.
- Schneebeli, M., T. U. Kaempfer, and S. A. Sokratov (2004), Time-lapse X-ray computed tomography of snow metamorphism: Instrumentation, *Geophys. Res. Abstr.*, *6*, Abstract EGU04-A-06109.
- Smith, R. C., et al. (1992), Ozone depletion: Ultraviolet radiation and phytoplankton biology in antarctic waters, *Science*, *255*, 952–959.
- Stammes, K., S. Tsay, W. Wiscombe, and K. Jayaweera (1988), Numerically stable algorithm for discrete-ordinate-method radiative transfer in multiple scattering and emitting layered media, *Appl. Opt.*, *27*, 2502–2509.
- Swamy, J. N., C. Crofcheck, and P. Mengüç (2007), A Monte Carlo ray tracing study of polarized light propagation in liquid foams, *J. Quant. Spectrosc.*, *104*, 277–287, doi:10.1016/j.jqsrt.2006.07.022.
- Takano, Y., and K. N. Liou (1995), Radiative transfer in cirrus clouds. Part III: Light scattering by irregular ice crystals, *J. Atmos. Sci.*, *52*, 818–837.
- Tape, W. (Ed.) (1994), *Atmospheric Halos, Antarct. Res. Ser.*, vol. 64, 143 pp., AGU, Washington, D. C.

- Thomas, W. H., and B. Duval (1995), Sierra Nevada, California, U.S.A., snow algae: Snow albedo changes, algal-bacterial interrelationships and ultraviolet radiation effects, *Arct. Alp. Res.*, *27*, 389–399.
- van Rietbergen, B., H. Weinans, R. Huiskes, and A. Odgaard (1995), A new method to determine trabecular bone elastic properties and loading using micromechanical finite-element models, *J. Biomech.*, *28*, 69–81.
- Vikhamar, D., and R. Solberg (2002), Subpixel mapping of snow cover in forests by optical remote sensing, *Remote Sens. Environ.*, *84*, 69–82.
- Warren, S. G. (1982), Optical properties of snow, *Rev. Geophys.*, *20*, 67–89.
- Warren, S. G. (1984), Optical constants of ice from the ultraviolet to the microwave, *Appl. Opt.*, *23*, 1206–1225.
- Warren, S. G., and W. J. Wiscombe (1980), A model for the spectral albedo of snow. II: Snow containing atmospheric aerosols, *J. Atmos. Sci.*, *37*, 2734–2745.
- Warren, S. G., R. E. Brandt, and P. O. Hinton (1998), Effect of surface roughness on bidirectional reflectance of Antarctic snow, *J. Geophys. Res.*, *103*, 25,789–25,807.
- Warren, S. G., R. E. Brandt, and T. C. Grenfell (2006), Visible and near-ultraviolet absorption spectrum of ice from transmission of solar radiation into snow, *Appl. Opt.*, *45*, 5320–5334.
- Wendler, G., and J. Kelley (1988), On the albedo of snow in Antarctica: A contribution to I.A.G.O. (Interaction Atmosphere-Glacier-Ocean), *J. Glaciol.*, *34*, 19–25.
- Wiscombe, W. J., and S. G. Warren (1980), A model for the spectral albedo of snow, I: Pure snow, *J. Atmos. Sci.*, *37*, 2712–2733.
- Wolff, E. W., A. E. Jones, T. J. Martin, and T. C. Grenfell (2002), Modeling photochemical NO_x production and nitrate loss in the upper snow-pack of Antarctica, *Geophys. Res. Lett.*, *29*(20), 1944, doi:10.1029/2002GL015823.

M. A. Hopkins, T. U. Kaempfer, and D. K. Perovich, Engineer Research and Development Center, Cold Regions Research and Engineering Laboratory, 72 Lyme Road, Hanover, NH 03755, USA. (mark.a.hopkins@erdc.usace.army.mil; thomas.kaempfer@erdc.usace.army.mil; donald.k.perovich@erdc.usace.army.mil)